Novel regulators of endosome dynamics, MHCII antigen presentation and chemosensitivity

Wijdeven, R.H.M.

Chapter 5:
USP54 is a novel regulator of cytoskeletal dynamics

Ruud H. Wijdeven[1,3,4], Ilana Berlin[1,3,4], George Jansen[2], Hans Janssen[3], Peter van Veelen[2], Jacques Neefjes[1,3]

[1] Department of Chemical Immunology, LUMC, Leiden, the Netherlands
[2] Department of Immunohematology and Blood Transfusion, LUMC, Leiden, the Netherlands.
[3] Department of Cell Biology, Netherlands Cancer Institute, Amsterdam, the Netherlands
[4] Contributed equally to this work

The endocytic pathway is critical for cellular organization, and spatiotemporally confined internalization from and recycling to specific plasma membrane sites is essential for the establishment of cell polarity. However, the molecular mechanisms underlying geographically restricted endosome transport and fusion are poorly understood. Here, we identified USP54 as an active DUB regulating cell-cell contact site integrity and endocytic transport. USP54 localizes to cell-cell contact sites and endosomes and traverses between these compartments. At these compartments, USP54 respectively co-localized and interacted with tight junction proteins including ZO-2 and select members of the HOPS tethering complex. Loss of USP54 decreased membrane localization of tight junction protein ZO-1 and induced peripheral re-localization and stabilization of microtubules, indicative of a cell polarity defect. Altered ZO-1 localization was also observed for HOPS depletion. Together, our data suggest that USP54 interacts with different complexes, including HOPS and tight junctions, to control trafficking of cell-cell contact proteins from endosomes to the cell surface and thus regulate the establishment of cell polarity.

The endocytic network is a highly dynamic arrangement of different carriers, each able to deliver or accept cargo from specific compartments. It serves as the primary means for communication with the extracellular environment, as well as with neighboring cells via physical contacts. These cell-cell contact sites are maintained by spatially restricted internalization and recycling of specific cell-cell contact proteins and are essential for the establishment of cell polarity (1, 2). Furthermore, the endocytic network controls specific cargo transport to the apical and basolateral sides of polarized cells, underscoring the diverse flavors of endosomes.
To identify novel regulators of the endocytic pathway, we used the results of an RNAi screen that we recently performed on the role of de-ubiquitinating enzymes (DUBs) in the MHCII pathway (Chapter 4). One of the hits was of particular interest, USP54. This mechanistically unstudied DUB is implicated in cell migration (3), a process involving cell polarization, and its loss yielded a strong clustering phenotype of the MHCII compartment, suggesting a function for this DUB in the transport dynamics of late endosomes. To assess whether this regulation is specific for MHCII or extends to the endocytic compartment as a whole, MelJuSo cells silenced for USP54 were analyzed by electron microscopy to determine the localization of membranous compartments. Strikingly, all endocytic vesicles, and even the mitochondria, clustered around the MTOC, leaving a nearly empty cytosolic peripheral space (Fig. S1a). Other cell types such as HeLa (cervical cancer) and U2OS (osteosarcoma) showed a more mixed phenotype, with cells showing strongly clustered organelles and other cells a more scattered phenotype. Thus, the clustering phenotype may be secondary to a different effect on cellular organization. Besides clustering of compartments, many cells lacking USP54 were bi- or multi-nucleated, suggesting defective mitosis or abscission (Fig. 1a). Consistent with this, the amount of cells with double the DNA-content was increased in these cells, both in MelJuSo and p53 pathway proficient U2OS cells (Fig. 1b and 1c). Given the presence of a Microtubule Interacting and Transport (MIT) domain in USP54 (Fig. 1d (4)), a microtubule-defect following USP54 silencing would be an option. Indeed, cells depleted for USP54 possessed

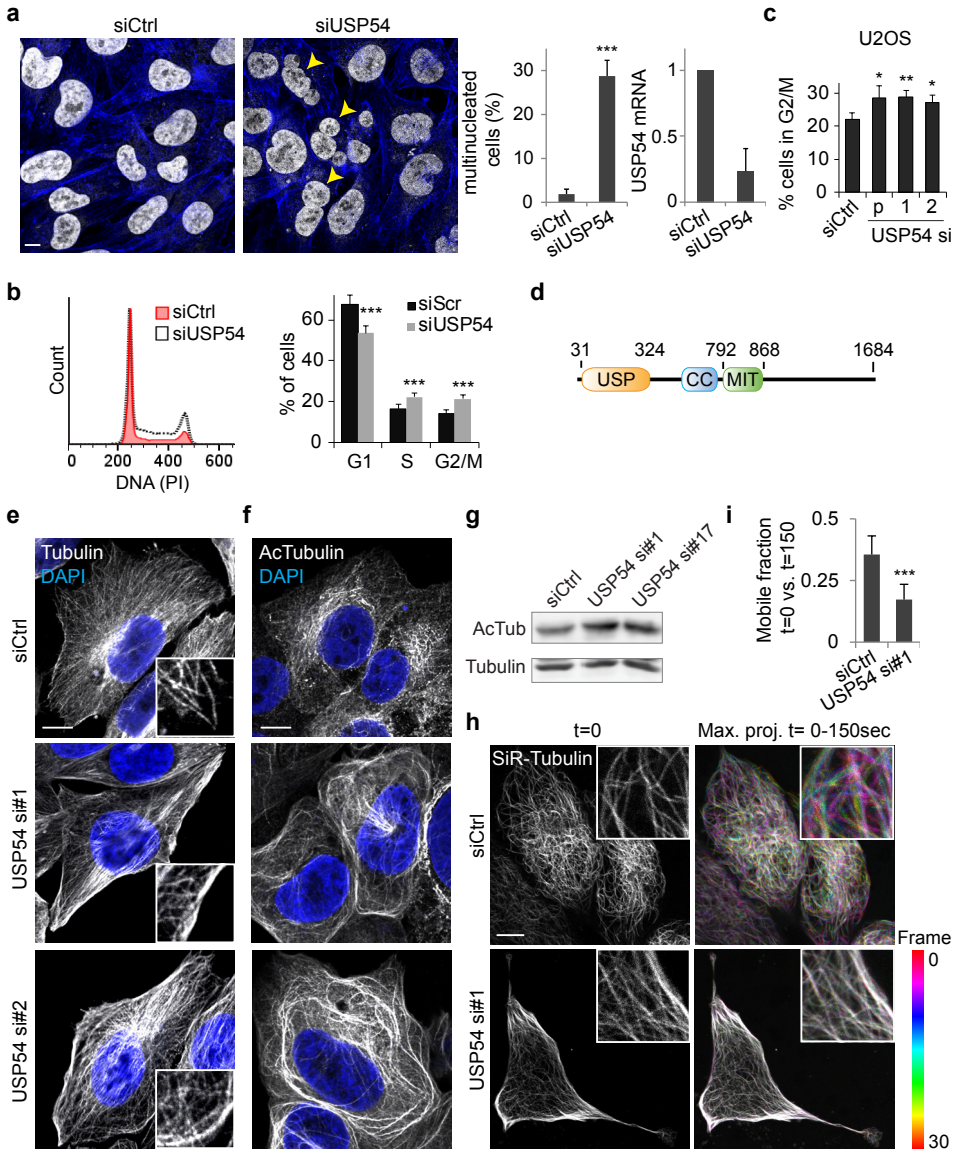

Figure 1: USP54 controls microtubule dynamics. *(A) MelJuSo cells transfected with the indicated siRNAs were fixed and stained with DAPI and Phalloidin (actin). Amount of cells with more than one DAPI-positive structure were counted for at least 50 cells per experiment, n=3. Right: silencing efficiency of USP54 was analyzed by qRT-PCR. (B) MelJuSo cells transfected with the indicated siRNAs were analyzed for cell cycle stage by flow cytometry using propidium iodide (PI). Left: representative FACS plot of PI intensity. Right: quantification of cells in different cell cycle stages. (C) U2OS cells transfected with the indicated siRNAs (USP54 pool of 4 siRNAs or specific siRNA sequences #1 and #2) were analyzed for cell cycle stage by flow cytometry using propidium iodide (PI). % of cells in G2/M phase was quantified. (D) USP54 domain structure. (E) MelJuSo transfected with the indicated siRNAs were fixed and stained with DAPI and Tubulin. (F) U2OS transfected with the indicated siRNAs were fixed and stained with DAPI and AcTubulin. Legend continues on next page*

a remarkably different microtubule structure, with a more peripheral localization of the bulk of the microtubules, sometimes following the edges of the cell (Fig. 1e and S1b). This was corroborated by an extended network of acetylated Tubulin (Fig. 1f), which labels relatively stable microtubules (5), implying these cells contain more static microtubules at the periphery. Overall levels of Acetylated Tubulin increased only marginally (Fig. 1g), hinting at a reorganization of the stable microtubule network. To address the mobility of the microtubule network, microtubule dynamics were followed using a fluorescent tubulin-binding compound (6) in cells either or not depleted for USP54. Again, we observed a massive microtubule network at the cellular edges and the microtubules were much more static compared to control cells, suggesting a defect in microtubule de-polymerization or docking at the plasma membrane (Fig. 1h and 1i). Together, these data establish a role for USP54 in cytoskeletal organization by influencing the dynamics of microtubules.

While containing a USP DUB-domain, USP54 was predicted to be catalytically inactive as it lacks a critical Histidine that assists the catalytic triad in conventional USP-domains (7). To assess whether this indeed prevented catalytic activity, we exposed USP54 to a DUB activity-based probe (8). Wild-type USP54, but not its counterpart missing the catalytic cysteine (C42S), reacted with the probe (Fig. 2a). However, the fraction of USP54 labelled by the activity-based probe was much lower than that for USP8 (and other active DUBs tested), suggesting slow reactivity, either because of the missing Histidine or because co-factors are required for full activity. Nevertheless, USP54 is a catalytically competent enzyme.

The presence of an MIT domain begged the question whether USP54 is in fact a microtubule-interacting protein that controls microtubule dynamics. However, we were unable to detect an interaction or co-localization between the MIT domain and tubulin. Rather, full-length USP54 exhibited three distinct localizations; the plasma membrane and more specifically cell-cell contact sites, actin filaments, and endosome-like structures (Fig. 2b). The cell-cell contact and endosome localization was primarily controlled by the C-terminal domain in USP54, since expression of the C-terminal 1432-1684 amino acids resembled the localization of the full length protein, albeit with a more spotted plasma membrane localization (Fig. 2c and 2d). These spots marked the locations where actin stress fibers between different cells were connected (Fig. 2e), usually the location of tight junctions (9). Time-lapse experiments showed that USP54 was immobile at these junctions for prolonged periods of time (Fig. 2f), suggesting USP54 is an integral part of the contact site. Fast, endosome-resembling mobility to and from the contact site was observed for USP54-positive structures (green arrows), indicating USP54 traffics to or from these

(G) Western blot analysis for the indicated markers on U2OS cells transfected with the indicated siRNAs. (H) Microtubules in U2OS cells transfected with the indicated siRNAs were followed in time using SIR-Tubulin. Left: still image at the start of the movie. Images were recorded for 150 seconds with an image every 5 seconds. Right: hyperstack of the individual frames, represented as a Spectrum image according to the legend on the right. Immobile microtubules appear white, mobile ones as a multicolor image. (I) Calculation of the percentage of mobile microtubule. Pearson's coefficient of the first and last image of the movies from (H) were calculated and coefficient was taken as percentage of immobile microtubule. Quantification of at least 10 cells over three independent experiments. For all experiments: bars indicate mean + SD from independent triplicate experiments. T-test statistical analysis ($p < 0.05$, ** $p < 0.01$, *** $p < 0.001$). For all experiments, bar = 10 µm.*

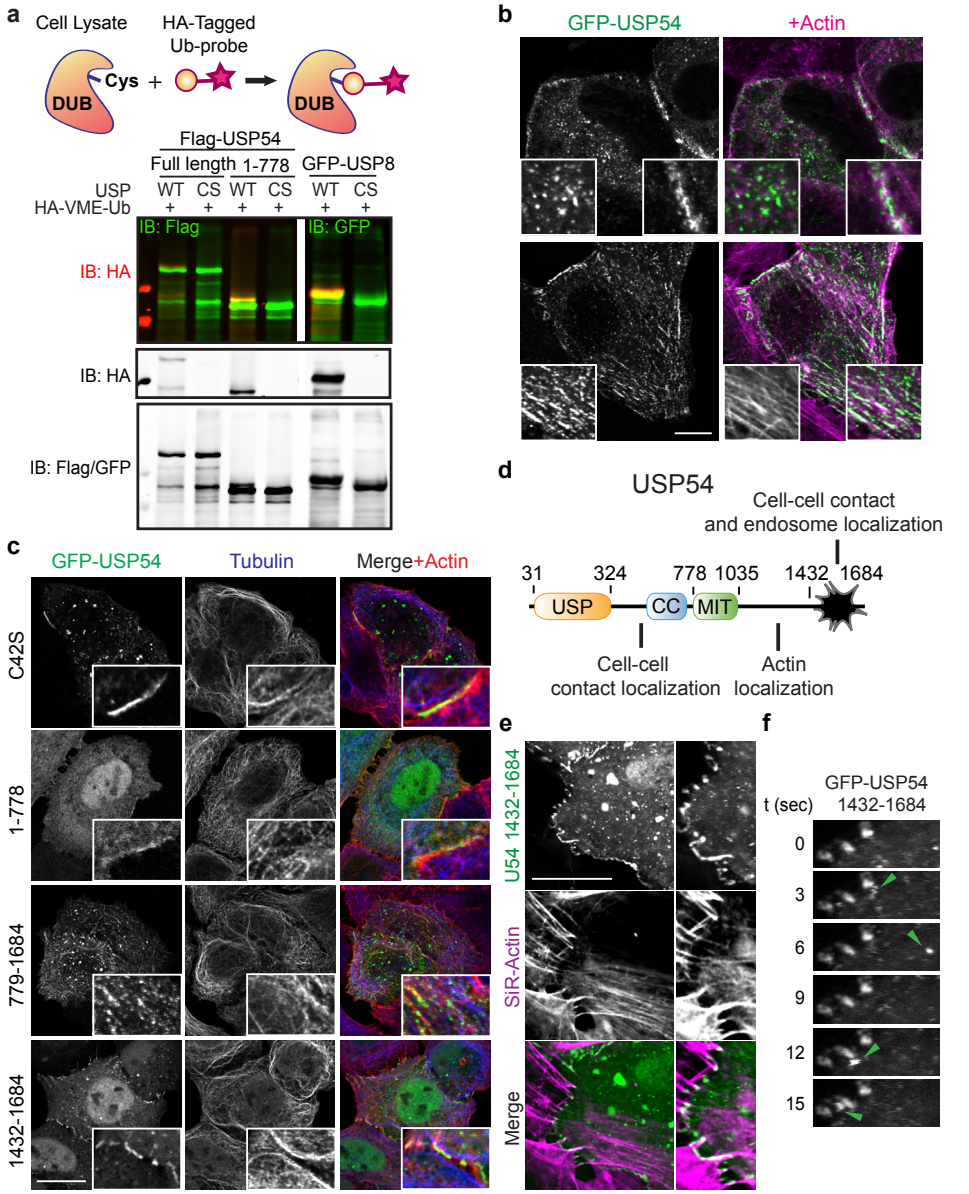

Figure 2: USP54 is a catalytically active DUB that localizes to membrane compartments. *(A) Ub-probe assay. Hek293T cells were transfected with the indicated plasmids (CS harbor a mutation in the catalytic site that renders the DUB inactive) and lysates were incubated with HA-VME-Ub for 30minutes. Samples were run on SDS-PAGE and analysed by western blot for HA (the probe) and Flag (the enzyme). (B) GFP-tagged USP54 was expressed in U2OS cells and cells were fixed and stained for actin. (C) GFP-tagged USP54 and mutants were expressed in HeLa cells and fixed and stained for actin and tubulin. (D) Overview of the localization determinants present in USP54 on the basis of experimets in (C) and (S2). (E) HeLa cells expressing GFP-USP54 1432-1684 were imaged together with SIR-Actin. Still image of a movie is shown. (F) Zoom-in of a movie made in (E), with different timepoints shown in separate frames. Green arrows indicate an endosome moving to or from the cell-cell contact site. For all experiments, bar = 10 µm.*

contact sites.
Extension of the C-terminal fragment, either 1035-1684 or 779-1684, redirected USP54 to actin fibers. This implies that the segment between the MIT domain and plasma membrane targeting domain likely interacts with actin-binding proteins (Fig. 2c and S2). The 1-778 and 1-1035 domains predominantly localized to the cytosol, although a small fraction localized to cell-cell contacts, indicating that the USP-domain and/or the coiled-coil domain contained some cell-cell contact localization determinants. Interestingly, cells ectopically expressing either the 1432-1684 or the catalytically inactive full-length enzyme (C42S) harbored a rounded microtubule structure resembling USP54 knockdown, suggesting that the catalytic activity of USP54 is required for its function, as well as the localization domain at the N-terminus. Thus, USP54 is an active DUB that localizes to cell-cell contact sites, endosomes and actin filaments. The different USP54 domains potentially regulate the interplay between these compartments.
Given its complex localization and domain structure, we set out to identify interacting proteins by immunoprecipitating different GFP-tagged USP54 domains and subjected interactors to mass spectrometry identification (Fig. 3a and 3b). This revealed that especially the coiled-coil domain and the C-terminal domain interact with a large array of proteins. The C-terminal fragment was associated with, among others, Plakoglobin/JUP/γ-Catenin, an integral component of desmosomes and adherens junctions, as well as several members of the HOPS complex (Fig. 3c). The extended C-terminal fragment, including the actin-localizing domain, isolated the actin-based motor proteins Myosin Heavy Chain 1 (MYH1), Myosin 1b and Myosin 1c, which could account for the actin localization. The coiled-coil domain precipitated a plethora of proteins, most notably: several members of tight and adherens junctions (most strongly ZO-1, ZO-2 and USP9x), multiple cilia proteins (predominantly IFT172), DOCK7 (a GEF for the RAC1 and CDC42 GTPases and involved in cell motility and polarity (10, 11)), HDAC6 (the deacetylase for αTubulin (12) and involved in adherens junction disassembly (13, 14)), SNX27 (a member of the sorting nexin family that mediates recycling of cargo from endosomes to the plasma membrane(15)), and STXBP4 (an inhibitor for STX4-mediated exocytosis (16)). Furthermore, strong co-immunoprecipitation was observed for several members of the 14-3-3 protein family of phosphorylation-binding proteins (17), suggesting that this USP54 domain harbors a phosphorylation site that is recognized by these proteins. Indeed, USP54 contains two canonical 14-3-3 binding RXXSXP sequences (18), and both localized in this isolated USP54-domain (amino acids 493-498 and 666-670). The USP-domain predominantly interacted with VCP/p97/TERA, a chaperone ATPase involved in the segregation of large protein complexes (19), and which also promotes sorting of Caveolin-positive endosomes towards the lysosome (20). Interestingly, this interaction occurred preferentially with the C42S variant. The MIT domain, besides its role in protein-protein interactions also known to interact with phospholipids such as PI3P and PI4P (21), interacted with the kinase DYRK1a and phosphatase PGAM5. Thus, we identified five domains in USP54, each with specific sets of interacting proteins.
During the formation of an epithelial cell layer, the establishment of apico-basal polarization is coupled to the formation of tight and adherens junctions, and this

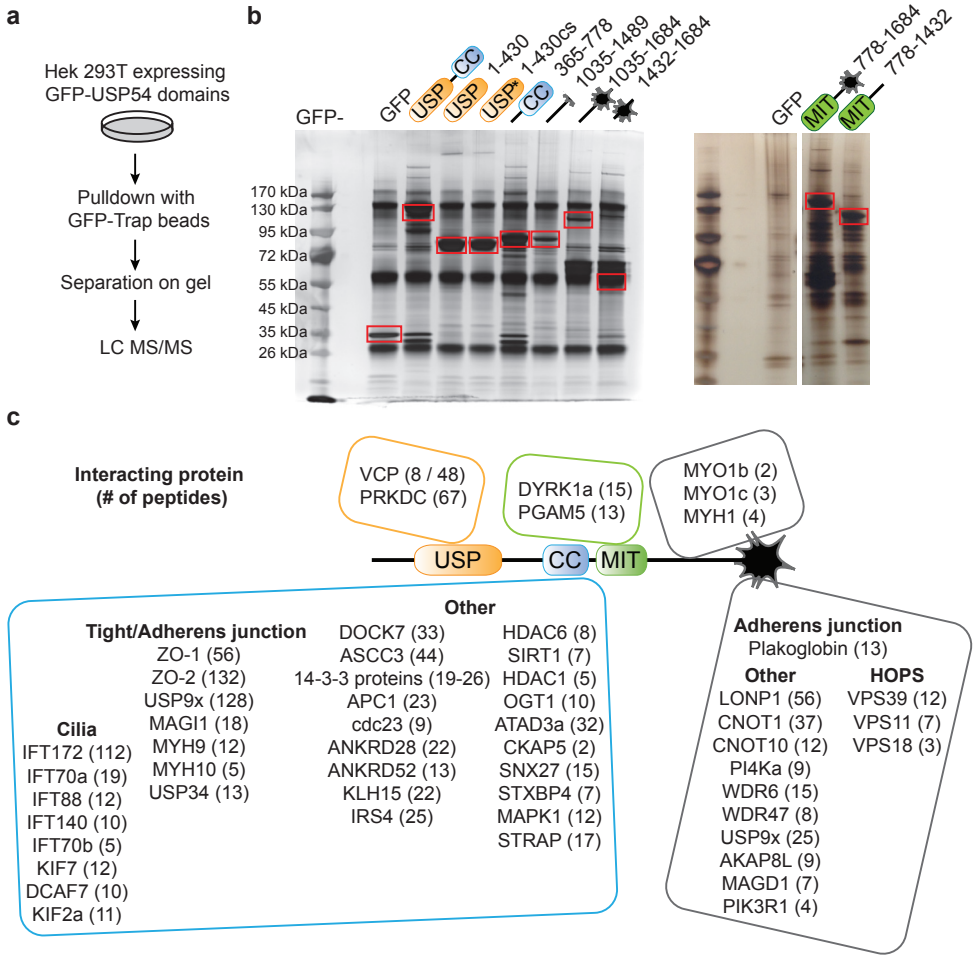

Figure 3: Identification of USP54-interacting proteins. *(A) Set-up of the mass spec experiment. Hek293T cells were transiently transfected with GFP or GFP-tagged USP54 domains and after lysis GFP was immunoprecipitated using GFP-Trap beads. Associated material was separated by SDS-PAGE and after silver staining the unique bands were subjected to MS/MS analysis. (B) Results of the silver stain and the constructs used. Red boxes indicate GFP-tagged proteins. (C) Selection of most relevant and abundant hits per domain, with the corresponding amount of peptides between brackets (). For VCP, number of peptides in respectively the active USP domain and inactive USP domain are shown. For fragment in between MIT and C-terminal domain, results from 1432-1684 were subtracted from the 1035-1684 domain. For MIT domain, 1035-1684 was subtracted from 779-1684.*

subsequently restructures the microtubule network towards a more peripheral texture (22-27). The strong immunoprecipitation of several tight / adherens junction proteins in conjunction with the described role for these junctions in cytoskeletal dynamics made us speculate that by interfering with the integrity of cell-cell contact sites or the formation of apical-basal lateral polarization, USP54 controls microtubule dynamics. USP54 at the cell-cell contact sites indeed co-localized with ZO-1, an integral member of both tight and adherens junctions (Fig. 4a). Co-immunoprecipitation experiments confirmed an interaction of USP54 with tight junction protein

ZO-2, but not ZO-1. Possibly ZO-1 interacts with ZO-2 and subsequently USP54. To address whether USP54 affects cell-cell contact site formation, we silenced USP54 and stained for ZO-1. Whereas in both U2OS and HeLa cells about half of the cells contained at least one ZO-1 positive cell-cell contact site, cells depleted for USP54 contained hardly any ZO-1 at the membrane (Fig. 4c and Fig. S3a). Most of the residual membranous ZO-1 was found on actin filaments running perpendicular to the plasma membrane (Fig. 4c, bottom inset). No effect was observed for the adherens junction members β-Catenin and y-Catenin (Fig. 4d and S3b), suggesting that USP54 controls the formation or stability of tight junctions but not adherens junctions.

Given the endosome-like localization of USP54, it could be involved in shuttling cargo from endosomes to cell-cell contact sites. The C-terminal domain of USP54 pulled-down three members of the HOPS complex, a tethering complex recruited to LE/Lys by Rab7 and Arl8b that mediates fusion and maturation of said endosomes (28-30), implying USP54 could be recruited to these structures. Indeed, USP54 co-localized with vesicle-localized VPS39, VPS11 and VPS18, but not with VPS41, another member of the HOPS core complex (Fig. 5a and S4a). In agreement with this and the mass spectrometry experiment, USP54 interacted with VPS39 and VPS18, but not with VPS41, or VPS33b, part of the HOPS-related VIPAR complex (31) (Fig. 5b), implying USP54 is recruited to only a segment of the HOPS complex. Interestingly, these VPS- and USP54-positive vesicles did not stain for CD63 (Fig. 5a), suggesting that the VPS-subunits interact with USP54 on a different type of endosome. Co-stainings with different endosomal markers did not show significant co-localization of USP54 with early endosomal Rab5, or to recycling endosomes marked by Rab11 and Transferrin receptor (Fig. S4b), although sometimes both endosomal structures were adjacent to each other and in close contact, as if somehow tethered. Whereas VPS11 and VPS18 are only known for their roles in the early endosomal CORVET and late endosomal HOPS tethering complexes, VPS39 can also be recruited by Rab2a to a specialized recycling endosome (32). Nevertheless, also Rab2a did not co-localize with USP54 (Fig. S4c). Thus, VPS39, VPS11 and VPS18 interact with the C-terminal tail of USP54 and co-localize on a yet undefined subset of endosomes (Fig. 5c).

To address whether VPS11, VPS18 and VPS39 are important for the function of USP54 in tight junction formation, we silenced the different subunits and addressed the localization of ZO-1. While membrane localization per se was not significantly impaired by VPS-knockdown, ZO-1 junctions often mislocalized to actin filaments perpendicular to the membrane or formed round structures, as if the junctions were ruptured in the middle and the cells detached from each other (Fig. 5d). Whereas not phenocopying USP54 silencing, both USP54 and the VPS-subunits appear to be involved in tight junction localization, possibly by acting in a large multi-protein complex.

Conclusions and future directions

Spatially confined internalization and recycling of cargo is crucial for the installment of polarity and cellular differentiation. However, the processes underlying this specific regulation are poorly understood. Here, we have identified USP54 as a novel fac-

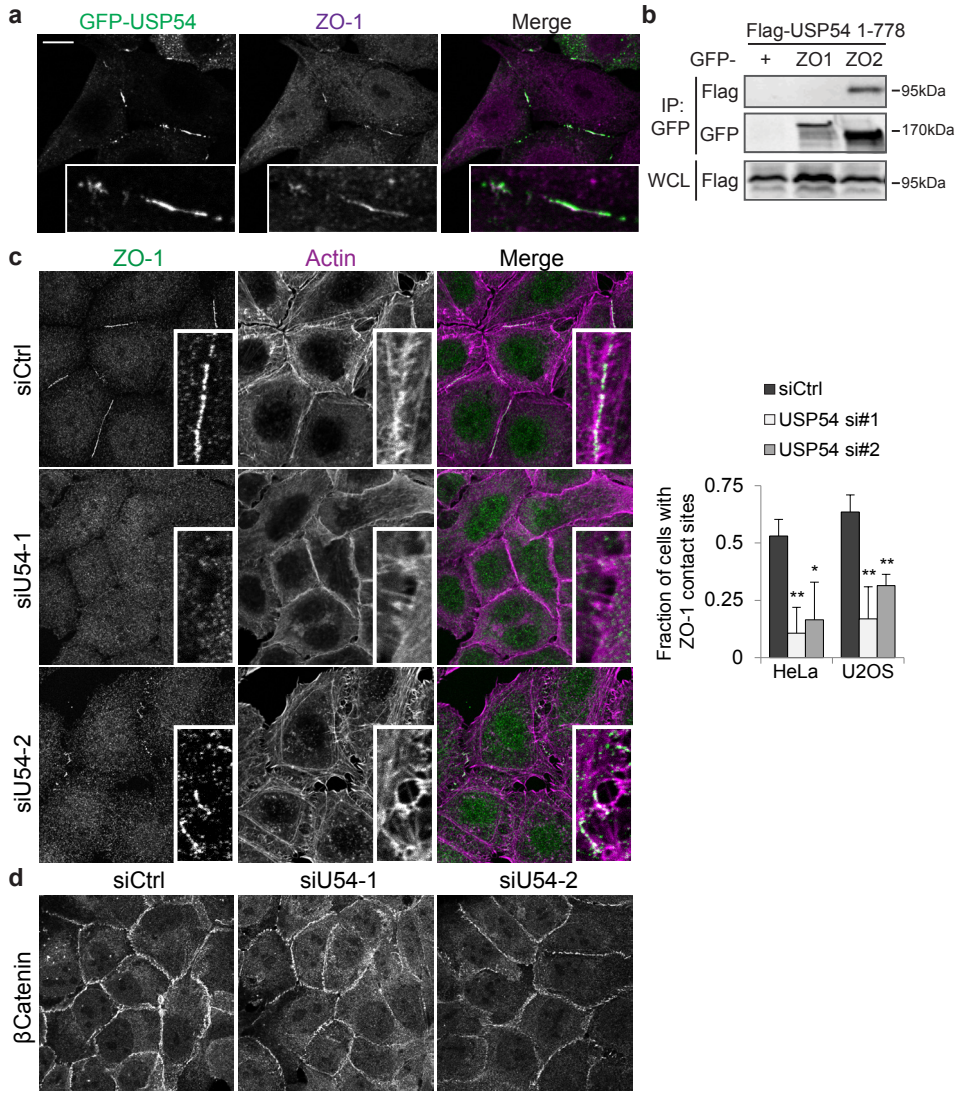

Figure 4: USP54 controls membrane localization of tight junction member ZO-1. *(A) USP54 co-localizes with ZO-1. HeLa cells transfected with GFP-USP54 were fixed and stained for ZO-1. (B) Co-immunoprecipitation for ZO-1 and ZO-2 with USP54. Indicated GFP-tagged construct was isolated from lysates of HEK293T cells co-overexpressing Flag-USP54 1-778 construct using GFP-Trap beads. Western blot filters were probed for isolated GFP-tagged proteins, and the associated Flag-USP54. (C) U2OS cells transfected with the indicated siRNAs were fixed and stained for ZO-1 and actin. Right: quantification of the amount of cells containing ZO-1 surface staining, quantified with at least 50 cells per experiment. (D) U2OS cells transfected with the indicated siRNAs were fixed and stained for β-Catenin. For all experiments, bar = 10 µm.*

tor that shuttles between endosomes and cell-cell contacts. USP54 is a catalytically competent DUB that resides at tight junction sites, actin filaments and endosomes. Functionally, loss of USP54 is accompanied by a shift in the microtubule structure towards a more peripheral and stable network, as well as loss in membrane localiza-

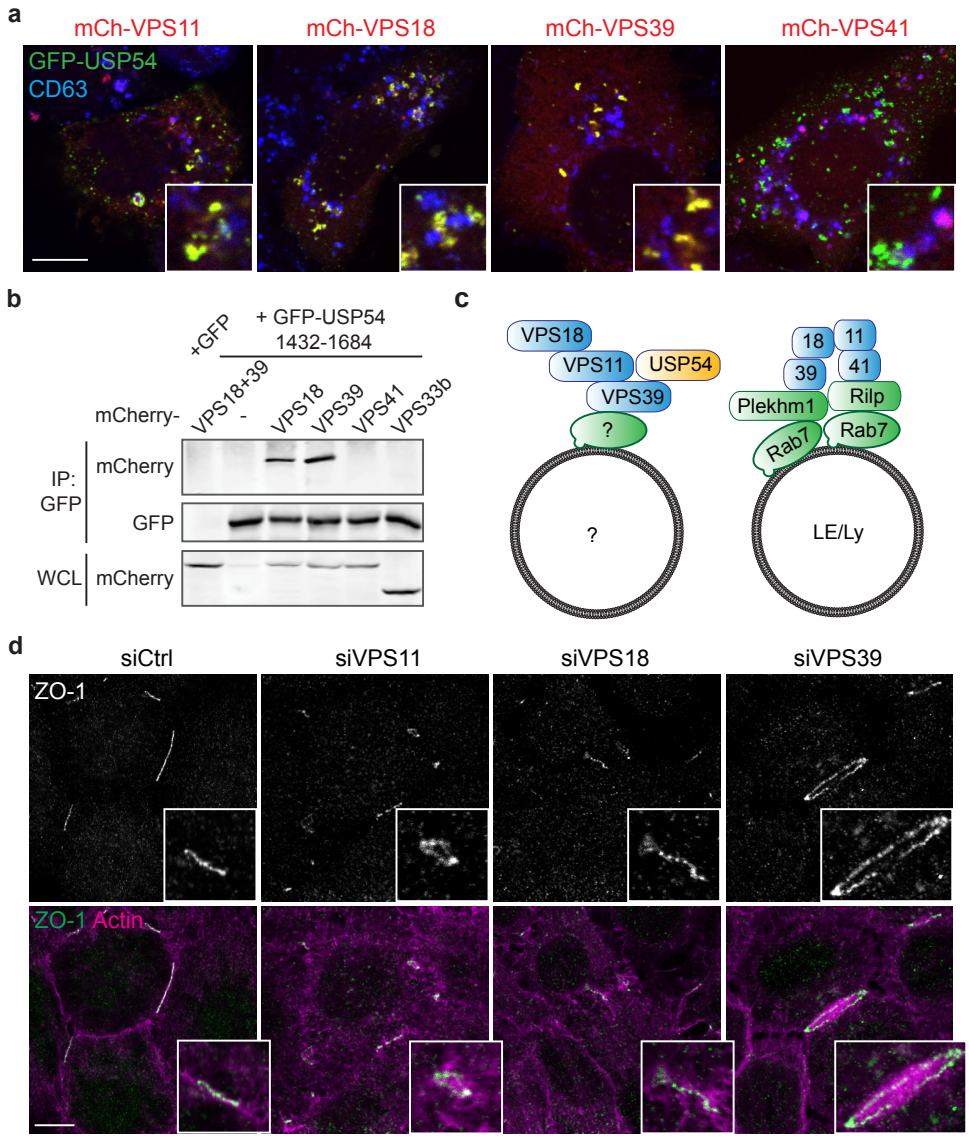

Figure 5: USP54 co-localizes and interacts with several subunits of the HOPS complex. *(A) USP54 co-localizes with select members of the HOPS complex. GFP-USP54 was co-transfected into HeLa cells with the indicated mCherry-VPS constructs, fixed and stained for CD63. (B) Co-immunoprecipitation in Hek293T cells for the indicated constructs. GFP-tagged USP54 1432-1684 was isolated using GFP-Trap beads and isolates were analyzed by western blot. Whole cell lysate (WCL) and IP samples were scanned on the same gel and are shown at the same scanning intensity. (C) Model for endosome recruitment of USP54 by HOPS subunits, versus the canonical HOPS recruitment to Rab7. (D) HeLa cells transfected with the indicated siRNAs were fixed and stained for ZO-1 and actin. For all experiments, bar = 10 µm.*

tion of junction protein ZO-1, suggesting USP54 plays a role in decisions regarding the polarity of cells.
The endocytic pathway contains a multitude of endosome sorting and recycling pathways, which are critical for cellular identity and tightly linked to cellular differentiation state and function. This is especially well described for polarized epithelial cells, where the integrity of the apical and basolateral sides are maintained by polarized endosomal recycling pathways (2). Specific recycling pathways control trafficking of endosomes towards the apical and basolateral sides, as well as towards the cilium and the lateral side where the tight junctions are formed (1). Our data suggest that USP54 localizes to a subset of recycling endosomes and is recycled to the plasma membrane at cell-cell contact sites. In agreement with this, cells grown individually, and thus lack cell-cell contact sites, display strictly endosomal or actin-localized USP54. These endosomes are not classical early or late endosomes, nor Rab2, Rab11 or Rab14 recycling endosomes. The mass spec experiment identified STXBP4/Synip as a possible USP54 interactor, which is an inhibitor of Syntaxin4- and Rab4-mediated recycling (16, 33, 34), suggesting that these endosomes could be Rab4+ recycling endosomes. Indeed, Rab4 and STX4 are implicated in recycling of tight and adherens junction proteins (35-37), and in polarized cells syntaxin-4 regulates recycling towards the basolateral membrane (38). Syntaxin-4 and STXBP4 are best studied for their role in recycling of the glucose uptake receptor GLUT4 in adipocytes (16, 39). Interestingly, a recent study showed that mice lacking USP54 are characterized by a strongly increased adipocyte mass (3), a phenotype that could arise from increased GLUT4-mediated glucose uptake by these cells (40-42). It would thus be interesting study the effect of USP54 on GLUT4 trafficking and STX4-mediated recycling of cargo.
USP54 has a very specific localization to different cellular structures, but what is its function? USP54 has been shown to be instrumental for cellular migration and is expressed at high levels in colon stem cells, but its actual function is unknown (3). Our data show that loss of USP54 resulted in altered microtubule organization, including enhanced formation or stabilization of peripheral microtubules, as well as the loss of tight junction protein ZO-1 from cell-cell contact sites. This altered microtubule cytoskeleton could arise from different sources. Firstly, USP54 could directly influence microtubule stability, for example by interacting with HDAC6, the microtubule deacetylase that was identified from the mass spec. Given its localization at the plasma membrane, it could mediate deacetylation specifically at these sites, which could lead to altered microtubule dynamics. However, given the limited role of microtubule acetylation in its stability (43-45), this is unlikely the primary function of USP54. Secondly, USP54 could recruit stabilizing or destabilizing factors, such as microtubule capping factors or interacting proteins. An interaction was found with microtubule capping enzyme CKAP5 (CH-TOG; identified by only 2 peptides), and some interactors or interacting complexes are linked to microtubule stabilizing or destabilizing factors, including DOCK7 (46), IFT proteins (47), and tight and adherens junctional proteins (24, 25). Alternatively, loss of USP54 perturbs the cellular differentiation and polarization process. Establishment of cell polarity is accompanied by changes in the microtubule network (26, 47), similar to that observed for USP54 knockdown. Furthermore, it instigates the formation of cell-cell contact sites, which

serve as physical barriers to separate the apical- and basolateral sides of polarized cells. Loss of ZO-1 membrane localization, but not adherens junction markers β- and γ-Catenin, after USP54 depletion suggests a defect in the formation of tight junctions which subsequently affects cell polarization. Besides junction proteins, another major group of USP54 interacting proteins identified by mass spec were cilia-associated factors, more specifically the intra-flagellar transport (IFT) proteins. Thus, it appears that USP54 localizes to multiple components of a polarized cell, the lateral side by virtue of the tight and adherens junctions, and the cilium via the IFT-proteins. Since the cells used in this study are incapable of full polarization and hardly contain cilia, it will be interesting to investigate the function of USP54 in polarity establishment in polarized cells such as HUVEC or MDCK. Our hypothesis would be that USP54 acts as a gatekeeper at different cellular sections to control their integrity (eg. Tight junctions and cilia), or regulates recycling of cargo specifically to these compartments.
Tight and adherens junctions are intimately connected to the actin cytoskeleton and actin connects junctions together to instigate tension formation between cells. Furthermore, endosome sorting and fission, as well as fusion with the plasma membrane, requires local actin (de)polymerization. Besides localizing to endosomes and cell-cell contacts, USP54 localizes to actin filaments via a domain at its C-terminus. Three actin-binding myosin motors were found to interact with this USP54 domain, Myosin 1b, 1c and MYH1. Of these, Myosin 1c is already known to interact with ZO-1 (48) and regulates GLUT4 exocytosis (49, 50) and adherens junction turnover (51), indicating a connection between actin and junction recycling, possibly controlled by USP54. Furthermore, USP54 interacts with DOCK7, a GEF for actin-polymerizing GTPases, and could hereby induce actin polymerization. Preliminary analysis indeed showed the appearance of polymerized actin on endosomes harboring full length catalytically inactive USP54, but not wild-type USP54 or the C-terminal tail alone, suggesting that the DUB domain inhibits actin polymerization. Via its slow catalytic activity, USP54 could act as a timer to regulate the turnover or activity of its cognate substrate. However, it is also possible that USP54 is strongly activated by substrate binding, for example by altering its catalytic fold. To gain full mechanistic understanding, it will be imperative to identify USP54 substrates using ubiquitin-proteomics. This would provide the framework for a more complete picture of the interacting proteins and substrates that in assembly determine the function of this fascinating DUB. Collectively, our work has identified an extensive set of interactors for the DUB USP54, arguing for a function in establishment of cell polarity and the recycling of specific endocytic cargo. Further research on this intriguing de-ubiquitinating enzyme will likely unravel novel and exciting biology, describing the regulation of cell polarity by the endocytic system.

Materials and methods

Cell culture and constructs

MelJuSo cells were cultured in IMDM supplemented with 10% FCS, U2OS, HeLa and Hek293T cells in DMEM with 10% FCS. The following constructs were obtained from addgene: GFP-ZO1 (#30313), GFP-ZO2 (#27422). GFP-RILP, mCherry-VPS and GFP-Rab constructs were described previously (29), as well as GFP-USP8 constructs (8). GFP-Rab2a was a kind gift from G. Scita (32). USP54 was ordered as a

custum synthesized gene and together with indicated truncation mutants re-cloned into the GFP-C1 and mRFP-C1 vectors.

Reagents and antibodies

For tubulin and actin staining respectively SIR-Tubulin and SIR-Actin (TeBu Bio) were used. Antibodies used: rabbit anti-GFP (1:1000), mouse anti-CD63 (1:500) and rabbit anti-CD63 (1:100) (all described in (29)), mouse anti-HA (Covance 16B12, 1:1000), rat anti-HA 3F10 (Roche, 1:200), rabbit anti-βCatenin, mouse anti-Tubulin and mouse anti-AcTubulin 6-11-B1 (both 1:100, Sigma), rabbit anti-ZO1, mouse anti-yCatenin A6 (all from Santa Cruz, both 1:100), actin was stained with Phalloidin-Alexa 647 (Life Technologies). Secondary antibodies (goat anti-mouse Alexa 405/488/568/647, goat anti-rabbit Alexa 488/568/647, donkey anti-goat Alexa 488/568, donkey anti-mouse Alexa 488/555/647 and donkey anti-rabbit Alexa 488/647) were purchased from Life Technologies and donkey anti-rat CF568 from Biotium (all 1:200).

Transfections

For expression studies, MelJuSo and HeLa cells were transfected using Effectene (Qiagen) according to the manufacturer's instructions. Cells were transfected one day before fixation or lysis. Hek293T cells were transfected using polyethylenimine (PEI). For siRNA mediated depletion, cells were reverse transfected with DharmaFECT transfection reagent #1 and 50 nM siRNA of the Human siGenome SMARTpool, Dharmacon, according to the manufacturer's protocol. siRNA sequences for USP54: #1 5'-GATAGAAGTTTGTCAGGTA-3' and #2 5'-GGTCACTGATAGAGCGCAA-3'. Briefly, siRNAs and DharmaFECT were mixed and incubated for 20 minutes in a culture well, after which cells were added and left to adhere (reverse transfection). Three days later, cells were fixed and stained or lysed for biochemical analysis.

Co-immunoprecipitation and Western blotting

For co-immunoprecipitation experiments, Hek293T cells were lysed in lysis buffer (0.5% NP-40, 5% glycerol, 150mM NaCl, 50mM Tris-HCl pH8.0, 5mM MgCl2 supplemented with complete EDTA-free Protease Inhibitor Cocktail (Roche)) and cleared by centrifugation. Lysates were incubated with GFP-Trap beads (Chromotek) or protein G-Sepharose 4 FF resin with the indicated antibodies and after incubation washed extensively with lysis buffer before addition of sample buffer (2% SDS, 10% glycerol, 5% β-mercaptoethanol, 60mM Tris-HCl pH 6.8 and 0.01% bromophenol blue).

For whole cell lysate analyses, cells were lysed directly in sample buffer. Proteins were separated by SDS-PAGE and transferred to Western Blot filters. Blocking of the filter and antibody incubations were done in PBS supplemented with 0.1 (v/v)% Tween and 5% (w/v) milk powder. Blots were imaged using the Odyssey Imaging System (LI-COR) or ChemiDoc (Bio-Rad).

Mass spectrometry

Samples from immune-precipitated GFP-tagged proteins were separated by SDS-PAGE and were silver stained (Invitrogen). Selected bands (and the same region in the GFP control lane as negative controls) were cut from the silver stained gel and subjected to reduction with dithiothreitol, alkylation with iodoacetamide and in-gel trypsin digestion using a Proteineer DP digestion robot (Bruker). Tryptic peptides were extracted from the gel, lyophilized, dissolved in 95/3/0.1 v/v/v water/acetonitril/formic acid and subsequently analyzed by online nanoHPLC MS/MS using an 1100

HPLC system (Agilent Technologies), as previously described (Meiring et al., 2002). Peptides were trapped at 10 µl/min on a 15mm column (100µm ID; ReproSil-Pur C18-AQ, 3 µm, Dr. Maisch GmbH) and eluted to a 200 mm column (50µm ID; Repro-Sil-Pur C18-AQ, 3 µm) at 150 nl/min. All columns were packed in house. The column was developed with a 30min gradient from 0 to 50% acetonitrile in 0.1% formic acid. The end of the nanoLC column was drawn to a tip (5-µm ID), from which the eluent was sprayed into a 7tesla LTQ-FT Ultra mass spectrometer (Thermo Electron). The mass spectrometer was operated in data-dependent mode, automatically switching between MS and MS/MS acquisition. Full scan MS spectra were acquired in the FT-ICR with a resolution of 25,000 at a target value of 3,000,000. The two most intense ions were then isolated for accurate mass measurements by a selected ion-monitoring scan in FT-ICR with a resolution of 50,000 at a target accumulation value of 50,000. Selected ions were fragmented in the linear ion trap using collision-induced dissociation at a target value of 10,000. In a post-analysis process, raw data were first converted to peak lists using Bioworks Browser software v3.2 (Thermo Electron), and then submitted to the Swissprot database version 51.6 (257,964 entries), using Mascot v. 2.2.04 (www.matrixscience.com) for protein identification. Mascot searches were with 2 ppm and 0.8 Da deviation for precursor and fragment mass, respectively, and trypsin as enzyme. Protein was finally sorted and compared using Scaffold software version 3.0.1 (www. proteomesoftware.com).

Ub-probe experiments

Assessment of catalytic activity was done using a HA-VME-Ub probe, which is covalently associated with a DUB when tries to cleave the modified thioester bond (8). Briefly, HEK293T cells were transfected with the indicated plasmids and lysed in mild lysis buffer (Tris pH 8.0 (50 mM), sucrose (250 mM), MgCl2 (5 mM), DTT (1 mM)) supplemented with CHAPS (0.5%) and NP40 (0.1%). After sonication, and centrifugation, the supernatant was incubated for 30minutes with 1µM HA-VME-Ub. After addition of sample buffer, cells were analyzed on an SDS-PAGE gel.

cDNA synthesis and qPCR

RNA isolation, cDNA synthesis and quantitative RT-PCR were performed according to the manufacturer's (Roche) instructions. Signal was normalized to GAPDH and calculated using the Pfaffl formula. Primers used for detection were: GAPDH fw: 5'-TGTTGCCATCAATGACCCCTT-3', GAPDH rv: 5'-CTCCACGACGTACTCAG-CG-3', HLA-DRα fw: 5'- -3', HLA-DRα rv: 5'- -3', IRF1 fw: 5'-GCACCAGTGATCT-GTACAAC-3', IRF1 rv: 5'-GCTCCTCCTTACAGCTAAAG-3', CIITA fw: 5'-CCTGCT-GTTCGGGACCTAAA-3, CIITA rv: 5'-GGATCCGCACCAGTTTGG-3', OTUD1 fw: 5'-CCTAGTATTTGGCTCAGTTGG-3', OTUD1 rv: 5'-TTGTCGTACTCTGGGT-TAGG-3'.

Confocal microscopy

Cells were seeded on coverslips, transfected 18 hours later and treated as indicated. 24 hrs later, cells were fixed in 3.7% formaldehyde for 10 min and permeabilized in ice-cold methanol (for LC3 stainings) for 2 minutes or in 0.1% Triton-X100 for 10 minutes. Alternatively, cells were fixed and permeabilized in ice-cold methanol for 2 minutes for Tubulin stainings. Staining was performed with the antibodies mentioned above and DAPI (Invitrogen) to stain DNA. Images were acquired using a Leica TCS SP5 confocal microscope (Leica Microsystems, Wetzlar, Germany) at 63x magnifi-

cation. For live-cell imaging, the microscope was equipped with a climate control chamber and cells were imaged for 3 minutes with ~12 frames per minute. Images were quantified using Image J plugin Jacob for Mander's or Pearson's coefficient calculations and processed using Adobe Photoshop and Illustrator.

Electron microscopy

Cells were fixed in Karnovsky fixative overnight. After washing with 0,1M Cacodylate buffer pH 7.2 the cells were postfixed with 1% Osmiumtetroxide, en-block stained with 0,5% uranylacetate (Ultrastain 1 from Leica, Austria) followed by dehydration series and embedding in Agar100/NMA/DDSA/BDMA (Aurion, the Netherlands). The sections were examined using a Tecnai12G2 microscope (FEI, the Netherlands).

Acknowledgements

We thank the NKI and LUMC microscopy facility, the NKI FACS facility and the NKI Robotics and Screening facility, with special thanks to Ben Morris for all his help with hit validations. Also, members of the Neefjes group for critical discussions, Nico Ong for developing electron micrographs, Lennert Janssen for help with cloning. This work was supported by the Institute of Chemical Immunology (ICI), an NWO Gravitation project funded by the Ministry of Education, Culture and Science of the government of the Netherlands and a European Research Council (ERC) advanced grant awarded to J.N.

References

1. E. Rodriguez-Boulan, I. G. Macara, Organization and execution of the epithelial polarity programme. Nature reviews. Molecular cell biology 15, 225-242 (2014).
2. D. M. Bryant, K. E. Mostov, From cells to organs: building polarized tissue. Nature reviews. Molecular cell biology 9, 887-901 (2008).
3. J. M. Fraile, D. Campos-Iglesias, F. Rodriguez, Y. Espanol, J. M. Freije, The deubiquitinase USP54 is overexpressed in colorectal cancer stem cells and promotes intestinal tumorigenesis. Oncotarget 7, 74427-74434 (2016).
4. D. J. Rigden, H. Liu, S. D. Hayes, S. Urbe, M. J. Clague, Ab initio protein modelling reveals novel human MIT domains. FEBS letters 583, 872-878 (2009).
5. L. Li, X. J. Yang, Tubulin acetylation: responsible enzymes, biological functions and human diseases. Cellular and molecular life sciences : CMLS 72, 4237-4255 (2015).
6. G. Lukinavicius et al., Fluorogenic probes for live-cell imaging of the cytoskeleton. Nat Meth 11, 731-733 (2014).
7. V. Quesada et al., Cloning and enzymatic analysis of 22 novel human ubiquitin-specific proteases. Biochemical and biophysical research communications 314, 54-62 (2004).
8. A. de Jong et al., Ubiquitin-based probes prepared by total synthesis to profile the activity of deubiquitinating enzymes. Chembiochem : a European journal of chemical biology 13, 2251-2258 (2012).
9. C. Zihni, M. S. Balda, K. Matter, Signalling at tight junctions during epithelial differentiation and microbial pathogenesis. Journal of cell science 127, 3401-3413 (2014).
10. Y. Zhou, J. L. Johnson, R. A. Cerione, J. W. Erickson, Prenylation and membrane localization of Cdc42 are essential for activation by DOCK7. Biochemistry 52, 4354-4363 (2013).
11. G. Gadea, A. Blangy, Dock-family exchange factors in cell migration and disease. European journal of cell biology 93, 466-477 (2014).
12. C. Hubbert et al., HDAC6 is a microtubule-associated deacetylase. Nature 417, 455-458 (2002).
13. Y. Li, X. Zhang, R. D. Polakiewicz, T. P. Yao, M. J. Comb, HDAC6 is required for epidermal growth factor-induced beta-catenin nuclear localization. The Journal of biological chemistry 283, 12686-12690 (2008).
14. J. Yu, M. Ma, Z. Ma, J. Fu, HDAC6 inhibition prevents TNF-alpha-induced caspase 3 activation

in lung endothelial cell and maintains cell-cell junctions. Oncotarget 7, 54714-54722 (2016).
15. F. Steinberg et al., A global analysis of SNX27-retromer assembly and cargo specificity reveals a function in glucose and metal ion transport. Nature cell biology 15, 461-471 (2013).
16. J. Min et al., Synip: a novel insulin-regulated syntaxin 4-binding protein mediating GLUT4 translocation in adipocytes. Molecular cell 3, 751-760 (1999).
17. Y. Aghazadeh, V. Papadopoulos, The role of the 14-3-3 protein family in health, disease, and drug development. Drug discovery today 21, 278-287 (2016).
18. C. Johnson et al., Bioinformatic and experimental survey of 14-3-3-binding sites. The Biochemical journal 427, 69-78 (2010).
19. H. Meyer, M. Bug, S. Bremer, Emerging functions of the VCP/p97 AAA-ATPase in the ubiquitin system. Nature cell biology 14, 117-123 (2012).
20. D. Ritz et al., Endolysosomal sorting of ubiquitylated caveolin-1 is regulated by VCP and UBXD1 and impaired by VCP disease mutations. Nature cell biology 13, 1116-1123 (2011).
21. N. Iwaya et al., MIT domain of Vps4 is a Ca2+-dependent phosphoinositide-binding domain. Journal of biochemistry 153, 473-481 (2013).
22. F. Martin-Belmonte, M. Perez-Moreno, Epithelial cell polarity, stem cells and cancer. Nature reviews. Cancer 12, 23-38 (2011).
23. C. Zihni, C. Mills, K. Matter, M. S. Balda, Tight junctions: from simple barriers to multifunctional molecular gates. Nature reviews. Molecular cell biology 17, 564-580 (2016).
24. L. A. Ligon, S. Karki, M. Tokito, E. L. Holzbaur, Dynein binds to beta-catenin and may tether microtubules at adherens junctions. Nature cell biology 3, 913-917 (2001).
25. M. N. Shahbazi et al., CLASP2 interacts with p120-catenin and governs microtubule dynamics at adherens junctions. The Journal of cell biology 203, 1043-1061 (2013).
26. D. A. Goldspink et al., The microtubule end-binding protein EB2 is a central regulator of microtubule reorganisation in apico-basal epithelial differentiation. Journal of cell science 126, 4000-4014 (2013).
27. D. Cohen, P. J. Brennwald, E. Rodriguez-Boulan, A. Musch, Mammalian PAR-1 determines epithelial lumen polarity by organizing the microtubule cytoskeleton. The Journal of cell biology 164, 717-727 (2004).
28. A. Spang, Membrane Tethering Complexes in the Endosomal System. Frontiers in cell and developmental biology 4, 35 (2016).
29. R. van der Kant et al., Late endosomal transport and tethering are coupled processes controlled by RILP and the cholesterol sensor ORP1L. Journal of cell science 126, 3462-3474 (2013).
30. D. Khatter et al., The small GTPase Arl8b regulates assembly of the mammalian HOPS complex on lysosomes. Journal of cell science 128, 1746-1761 (2015).
31. R. van der Kant et al., Characterization of the mammalian CORVET and HOPS complexes and their modular restructuring for endosome specificity. The Journal of biological chemistry 290, 30280-30290 (2015).
32. H. Kajiho et al., RAB2A controls MT1-MMP endocytic and E-cadherin polarized Golgi trafficking to promote invasive breast cancer programs. EMBO reports 17, 1061-1080 (2016).
33. L. Li, W. Omata, I. Kojima, H. Shibata, Direct interaction of Rab4 with syntaxin 4. The Journal of biological chemistry 276, 5265-5273 (2001).
34. L. J. Foster, A. Klip, Mechanism and regulation of GLUT-4 vesicle fusion in muscle and fat cells. American journal of physiology. Cell physiology 279, C877-890 (2000).
35. A. I. Ivanov, A. Nusrat, C. A. Parkos, Endocytosis of epithelial apical junctional proteins by a clathrin-mediated pathway into a unique storage compartment. Molecular biology of the cell 15, 176-188 (2004).
36. M. Matsuda, A. Kubo, M. Furuse, S. Tsukita, A peculiar internalization of claudins, tight junction-specific adhesion molecules, during the intercellular movement of epithelial cells. Journal of cell science 117, 1247-1257 (2004).
37. J. Torres, H. M. Funk, M. M. Zegers, M. B. ter Beest, The syntaxin 4 N terminus regulates its basolateral targeting by munc18c-dependent and -independent mechanisms. The Journal of biological chemistry 286, 10834-10846 (2011).
38. E. Reales, N. Sharma, S. H. Low, H. Folsch, T. Weimbs, Basolateral sorting of syntaxin 4 is dependent on its N-terminal domain and the AP1B clathrin adaptor, and required for the epithelial cell polarity. PloS one 6, e21181 (2011).
39. H. Yu, S. S. Rathore, J. Shen, Synip arrests soluble N-ethylmaleimide-sensitive factor at-

tachment protein receptor (SNARE)-dependent membrane fusion as a selective target membrane SNARE-binding inhibitor. The Journal of biological chemistry 288, 18885-18893 (2013).
40. P. R. Shepherd et al., Adipose cell hyperplasia and enhanced glucose disposal in transgenic mice overexpressing GLUT4 selectively in adipose tissue. The Journal of biological chemistry 268, 22243-22246 (1993).
41. M. A. Herman et al., A novel ChREBP isoform in adipose tissue regulates systemic glucose metabolism. Nature 484, 333-338 (2012).
42. J. M. Rutkowski, J. H. Stern, P. E. Scherer, The cell biology of fat expansion. The Journal of cell biology 208, 501-512 (2015).
43. S. C. Howes, G. M. Alushin, T. Shida, M. V. Nachury, E. Nogales, Effects of tubulin acetylation and tubulin acetyltransferase binding on microtubule structure. Molecular biology of the cell 25, 257-266 (2014).
44. J. Asthana, S. Kapoor, R. Mohan, D. Panda, Inhibition of HDAC6 deacetylase activity increases its binding with microtubules and suppresses microtubule dynamic instability in MCF-7 cells. The Journal of biological chemistry 288, 22516-22526 (2013).
45. K. Sadoul, S. Khochbin, The growing landscape of tubulin acetylation: lysine 40 and many more. The Biochemical journal 473, 1859-1868 (2016).
46. M. Watabe-Uchida, K. A. John, J. A. Janas, S. E. Newey, L. Van Aelst, The Rac activator DOCK7 regulates neuronal polarity through local phosphorylation of stathmin/Op18. Neuron 51, 727-739 (2006).
47. A. A. Bizet et al., Mutations in TRAF3IP1/IFT54 reveal a new role for IFT proteins in microtubule stabilization. Nature communications 6, 8666 (2015).
48. S. E. Goldblum et al., The active Zot domain (aa 288-293) increases ZO-1 and myosin 1C serine/threonine phosphorylation, alters interaction between ZO-1 and its binding partners, and induces tight junction disassembly through proteinase activated receptor 2 activation. FASEB journal : official publication of the Federation of American Societies for Experimental Biology 25, 144-158 (2011).
49. M. F. Yip et al., CaMKII-mediated phosphorylation of the myosin motor Myo1c is required for insulin-stimulated GLUT4 translocation in adipocytes. Cell metabolism 8, 384-398 (2008).
50. A. Bose et al., Unconventional myosin Myo1c promotes membrane fusion in a regulated exocytic pathway. Molecular and cellular biology 24, 5447-5458 (2004).
51. H. Tokuo, L. M. Coluccio, Myosin-1c regulates the dynamic stability of E-cadherin-based cell-cell contacts in polarized Madin-Darby canine kidney cells. Molecular biology of the cell 24, 2820-2833 (2013).

Supplementary Figures

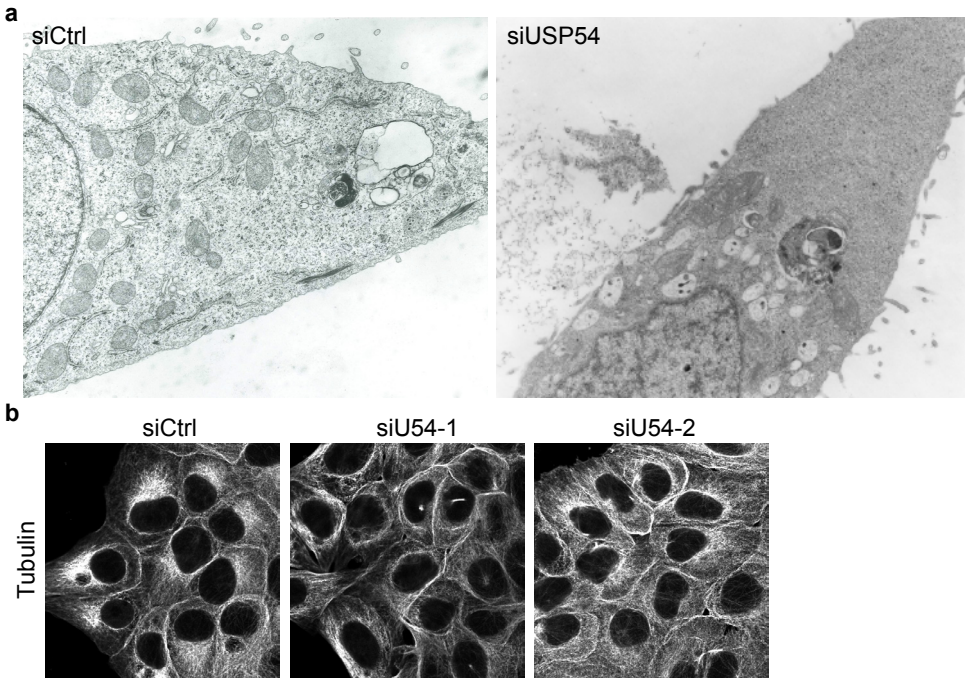

Supplementary Figure S1: USP54 controls microtubule dynamics. *(A) Electron micrograph of Mel-JuSo cells transfected with the indicated siRNAs. Note the absence of peripheral endosomal structures in the siUSP54 condition. (B) siRNA transfected U2OS cells were fixed and stained for the indicated markers.*

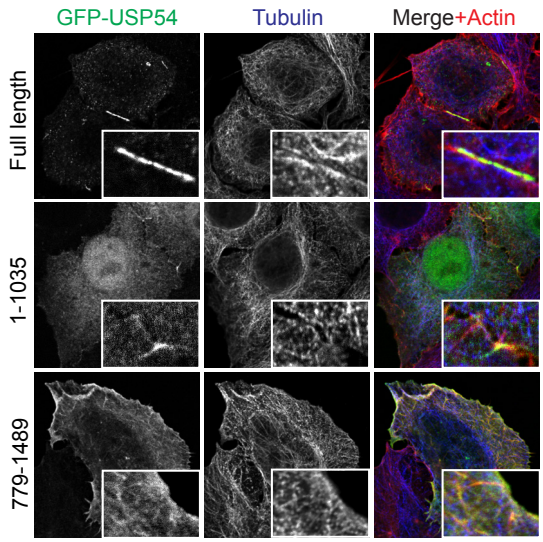

Supplementary Figure S2: localization determinants for USP54. *HeLa cells were transfected with the indicated GFP-tagged USP54 constructs, fixed and stained for Actin and Tubulin.*

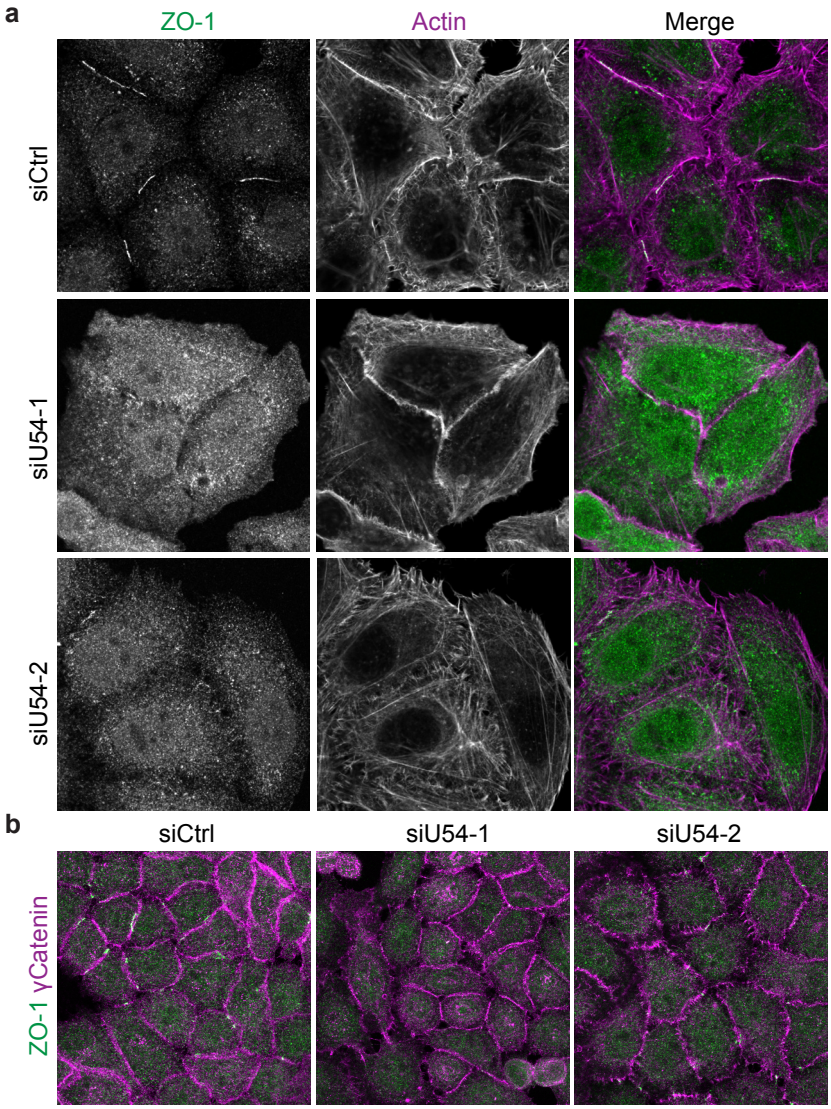

Supplementary Figure S3: USP54 mediates ZO-1 membrane localization. *(A) siRNA transfected HeLa cells were stained for the indicated markers. (B) siRNA transfected HeLa cells were stained for the indicated markers. Image represents maximum Z-projection of multiple images.*

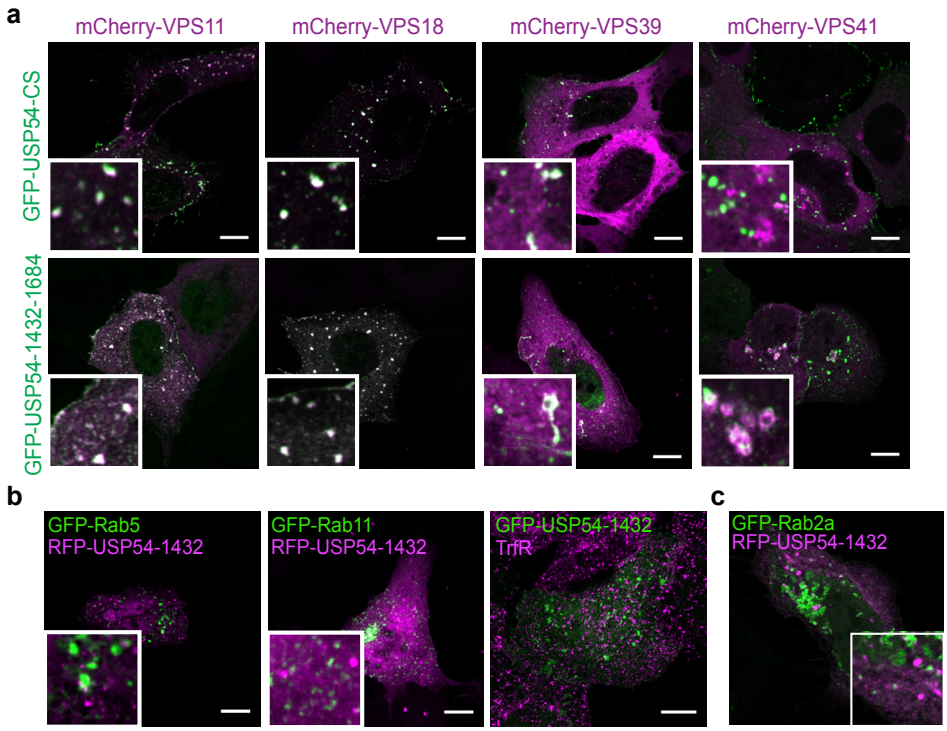

Supplementary Figure S4: USP54 co-localizes with members of the HOPS complex. *(A) HeLa cells transfected with the indicated constructs were fixed and imaged. (B) HeLa cells transfected with the indicated constructs were fixed, stained and imaged. (C) HeLa cells transfected with GFP-Rab2a, RFP-USP54 1432-1684 and Flag-VPS39 were fixed, stained and imaged. For all experiments, bar = 10 µm.*